Journal of Hazardous Materials 445 (2023) 130608

Contents lists available at ScienceDirect

Journal of Hazardous Materials

journal homepage: www.elsevier.com/locate/jhazmat

Research Paper

Identification and quantification of Cr, Cu, and As incidental nanomaterials derived from CCA-treated wood in wildland-urban interface fire ashes

Mahbub Alam [a], Talal Alshehri [a,b], Jingjing Wang [a], Sheryl A. Singerling [c], Charles N. Alpers [d], Mohammed Baalousha [a,*]

[a] Center for Environmental Nanoscience and Risk, Department of Environmental Health Sciences, Arnold School of Public Health, University of South Carolina, Columbia, South Carolina, United States

[b] Environmental Health Department, College of Public Health, Imam Abdulrahman Bin Faisal University, Dammam 31441, Saudi Arabia

[c] National Center for Earth and Environmental Nanotechnology Infrastructure (NanoEarth), Institute for Critical Technology and Applied Science, Virginia Polytechnic Institute and State University, Blacksburg, Virginia, United States

[d] US Geological Survey, California Water Science Center, 6000 J Street, Sacramento, CA 95819, United States

HIGHLIGHTS

- Chromium, copper, and arsenic concentrations in WUI fire ash were determined.
- The composition of Cr, Cu, and As INMs in WUI fire ash were determined.
- Original and transformed Cr, Cu, and As-bearing INMs were detected in WUI fire ash.
- The source of Cr, Cu, and As-bearing INMs in WUI fire ashes is treated wood.

GRAPHICAL ABSTRACT

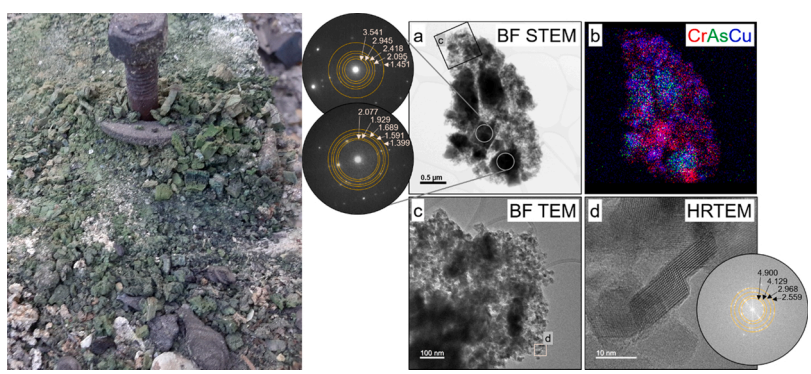

ARTICLE INFO

Editor: Lingxin Chen

Keywords:
Chromated Copper Arsenate
Wildland-urban interface fires
Incidental nanomaterials
Chromium, Copper, and Arsenic
Phase identification

ABSTRACT

In addition to the combustion of vegetation, fires at the wildland-urban interface (WUI) burn structural materials, including chromated copper arsenate (CCA)-treated wood. This study identifies, quantifies, and characterizes Cr-, Cu-, and As-bearing incidental nanomaterials (INMs) in WUI fire ashes collected from three residential structures suspected to have originated from the combustion of CCA-treated wood. The total elemental concentrations were determined by inductively coupled plasma-time of flight-mass spectrometry (ICP-TOF-MS) following acid digestion. The crystalline phases were determined using transmission electron microscopy (TEM), specifically using electron diffraction and high-resolution imaging. The multi-element single particle composition and size distribution were determined by single particle (SP)-ICP-TOF-MS coupled with agglomerative hierarchical clustering analysis. Chromium, Cu, and As are the dominant elements in the ashes and together account for 93%, 83%, and 24% of the total mass of measured elements in the ash samples. Chromium, Cu, and As phases, analyzed by TEM, most closely match CrO_3, CrO_2, eskolaite (Cr_2O_3), $CuCrO_2$, $CuCr_2O_4$, $CrAs_2O_6$, As_2O_5, AsO_2, claudetite (As_2O_3, monoclinic), or arsenolite (As_2O_3, cubic), although a bona

* Corresponding author.
E-mail address: mbaalous@mailbox.sc.edu (M. Baalousha).

https://doi.org/10.1016/j.jhazmat.2022.130608
Received 26 September 2022; Received in revised form 25 November 2022; Accepted 12 December 2022
Available online 15 December 2022

fide phase identification for each particle was not always possible. These phases occur predominantly as heteroaggregates. Multi-element single particle analyses demonstrate that Cr occurs as a pure phase (*i.e.,* Cr oxides) as well as in association with other elements (*e.g.,* Cu and As); Cu occurs predominantly in association with Cr and As; and As occurs as As oxides and in association with Cu and Cr. Several Cr, Cu, and As clusters were identified and the molar ratios of Cr/Cu and Cr/As within these clusters are consistent with the crystalline phases identified by TEM as well as their heteroaggregates. These results indicate that WUI fires can lead to significant release of CCA constituents and their combustion-transformed by-products into the surrounding environment. This study also provides a method to identify and track CCA constituents in environmental systems based on multi-element analysis using SP-ICP-TOF-MS.

1. Introduction

Fire (*i.e.,* wildfire and controlled fire) is a common phenomenon worldwide [7], affecting around 3–5 million km^2 annually, burning forest materials, structures, houses, and vegetated land [64]. Wildfires are a frequent phenomenon across the United States, which has witnessed a rapid increase in the area burned by wildfires by approximately 780 km^2 per year between 1991 and 2020, with the 2020 fire season consuming a record 41,000 km^2 of wildland [68]. Wildfires have become more destructive in recent years in the western United States, particularly in California, due to the dominance of flammable trees, shrubs, and grasses, topography, rising temperatures from climate change, and the increased population living in proximity to wildland vegetation in areas known as the wildland-urban interface (WUI) [46, 69]. Wildfires are most pronounced and devastating at the WUI, where houses and wildland vegetation intermingle [46,56]. This issue is of particular concern given the rapid growth of regions that qualify as the WUI. Between 1990 and 2010, the WUI grew rapidly in the United States in terms of both land area (from 581,000 to 770,000 km^2; 33%) and number of new houses (from 30.8 to 43.4 million; 41%) [56]. Additionally, the number of houses within the perimeter of recent wildfires (1990–2015) increased from 177,000 in 1990–286,000 houses in 2010 [56]. Consequently, the number of structures burned in WUI fires has increased from around 5200 structures, including 3500 houses in 2011, to 18,000 structures, including 9600 houses in 2020 (approximate increases of 246% for structures and 174% for houses burned in 10 years) [30,68].

Increases in wildfire frequency, size, severity, and encroachment into the built environment result in increased emissions of contaminants of emerging concern—metals and metalloids [67], organic contaminants [67], incidental nanomaterials [2], magnetic nanomaterials [4], as well as other types of contaminants. These contaminants likely pose risks to drinking water supplies and aquatic organisms [10,23,8]. Although several studies have investigated the types and concentrations of contaminants released from wildfires [13,14], studies reporting the nature and concentrations of contaminants released from WUI fires remain limited. Fires at the WUI transform and release chemicals used in construction materials into the atmosphere and ashes that remain on the ground. One such chemical is chromated copper arsenate (CCA), which has been used as a wood preservative or in pesticides since the 1930 s [15,45,26,27,31,58]. CCA is a waterborne salt that consists of a mixture of chromium trioxide (CrO_3, 47.5%), copper oxide (CuO, 18.5%), and arsenic pentoxide (As_2O_5, 34%) mixed in water [15,17,48]. Depending on the intended application, wood is treated to CCA retention levels between 4.0 and 40 kg m^{-3} [44], with most CCA-treated wood marketed to customers with a retention level of 6.4 kg m^{-3} [67]. CCA is the principal wood preservative in many countries [6]. The usage of CCA has greatly increased since the 1970 s, especially for residential applications—such as decks, picnic tables, landscaping timbers, fencing, patios, walkways, boardwalks, and playground structures— [27,31,6] until it was phased out of use in 2003 [63]. For instance, approximately 75,000 metric tons of CCA (oxide basis) were used in 2000 in North America and 15,000 metric tons in Europe. In December 2003, CCA manufacturers voluntarily discontinued manufacturing CCA-treated wood products for homeowner uses [63]. However, the U.S. Environmental Protection Agency (EPA) does not require the removal of existing structures made with CCA-treated wood [48,67]. Therefore, CCA is still considered a source of environmental contamination and health concern [48].

Several studies have investigated the concentrations of Cr, Cu, and As and the transformation of CCA constituents in ashes generated by controlled burning of CCA-treated wood [24,27,39,44,52,53,67]. During the incineration of CCA-treated wood, Cr and Cu compounds mostly remain in the ash as water-insoluble solids while As compounds change to volatile arsenic or arsenious acids [24]. Residual ash has been shown to contain high concentrations of Cr (~16%), Cu (~9%), and As (~8%), along with percent levels of Ca, Si, Fe, Al, Mg, and K [67]. A comparison of the residual ash and fly ash (*e.g.,* the fine particle ash that rises up with the flue gases) compositions suggest that between 11% and 14% of the As partitions into the fly ash while over 99% of the Cr and Cu partition into the residual ash [67]. These behaviors are consistent with the relatively low boiling temperature of As (615 °C) and the high boiling temperatures of Cu and Cr (2567 and 2672 °C) [57]. The dominant phases identified in the residual ash of CCA treated wood include: $CuCrO_2$, $CuCr_2O_4$, Cr_2O_3, $MgCr_2O_4$, and $K_3Na(CrO_4)_2$ (an analogue of aphthitalite, a sulfate mineral) for Cr; $CuCrO_2$, $CuCr_2O_4$, and $Cu_3(AsO_4)_2$ for Cu; and arsenate phases with Cu and Cr as well as As_2O_3 for As [39].

Previous studies used transmission electron microscopy (TEM), X-ray diffraction (XRD), and X-Ray absorption spectroscopy (XAS) to investigate the phases and oxidation states of CCA in treated wood and treated wood ash [24,67]. Although these methods provide structural information, TEM lacks statistical power as few particles can be practically measured, and XRD and XAS do not provide information on primary particle and aggregate size distributions. Single particle inductively coupled plasma-time of flight mass spectrometry (SP-ICP-TOF-MS) is a promising technique in nanometrology that enables the determination of the masses of all elements in a single particle in addition to particle sizes and number concentrations [29,37,47,62]. SP-ICP-TOF-MS measures all elements in a particle simultaneously and, when coupled with phase identification using TEM, allows for identification of the elemental composition, size distribution, and number concentrations of NMs.

This study identifies, quantifies, and characterizes the properties of Cr, Cu, and As in WUI fire ashes collected from three residential structures following the 2020 LNU Lightning Complex Fire in California and suspected to have originated from the combustion of CCA-treated wood. To this end, the three fire ashes were characterized for total bulk elemental concentrations, multi-element single particle composition, size distribution, and crystalline phase identification using SP-ICP-TOF-MS and TEM.

2. Materials and methods

2.1. Sampling location and sample collection

A detailed description of the LNU Lightning Complex Fire is provided elsewhere [2,4]. Briefly, this fire burned 1470 km^2 and destroyed 1491 structures in Colusa, Lake, Napa, Sonoma, Solano, and Yolo Counties,

approximately 60 km west of Sacramento, California between August 17 and October 2, 2020 (Fig. S1). Within the fire perimeter, the distribution of burn severity (area%) was 12% low, 39% moderate, and 49% high [4]. Land use in the fire perimeter consisted of 57% shrub/scrub, 19% herbaceous, 12% evergreen forest, and 1.4% developed. Fire ash samples were collected from three burned houses in October 2020 following the LNU Lightning Complex Fire. Approximate locations of the three houses are given in Table S1 and shown in Fig. S1. The burn severity in the vicinity of these sampling locations was moderate to high; each of the houses was completely burned. Sample A24 is a dark green ash collected from a building foundation (Figs S2a and S2d). Sample A96 is a light gray ash with some green color collected from a burned house (Fig. S2b). Sample A125 is olive green ash collected from another foundation with some visible yellow crystals (Fig. S2c). Ash samples were collected with disposable plastic scoops and placed into zippered plastic bags. All samples were collected prior to any precipitation.

2.2. Digestion and metal analysis

Ash samples were homogenized using a mortar and a pestle, sieved through a 2 mm pore size mesh nylon sieve (Zhangxing Instrument, Hangzhou, Zhejiang, China), and digested for total metal concentration analysis according to the methods described elsewhere [2]. Briefly, 100 mg of the sieved ashes were weighted and placed into a polytetrafluoroethylene (PTFE) digestion vessel. Digestion reagents were added to each sample, standard reference materials, and procedural blanks in the following order: 9 mL of distilled HNO_3, 3 mL of distilled HF, and 2 mL of H_2O_2. The acid digestion was performed in a Multiwave microwave (Multiwave Pro, Anton Paar, Graz, Austria) at a constant power of 1500 W for 60 min preceded by a 15-minute ramping time to reach the desired power. The digestate was then evaporated in two steps using the same microwave system to remove non-reacted HF. The first evaporation was performed with 10 min of ramping time followed by 9 min of holding time at 1500 W. Then, 3 mL of distilled HNO_3 were added into the vessel to dissolve any insoluble fluoride salts, and the second evaporation was performed with 10 min of ramping time followed by 3 min of holding time at 1500 W. The digested samples were then diluted in 10% HNO_3 (trace metal grade, Fisher Chemical, Fair Lawn, NJ, USA) and stored until total metal analysis.

Total metal concentrations were determined using an inductively coupled plasma-time of flight-mass spectrometer (ICP-TOF-MS, TOFWERK, Thun, Switzerland). Mass spectra calibration and routine tuning were performed prior to analysis every day to achieve maximum sensitivity. Elemental concentration calibration was established using a series of ionic standards prepared in 1% HNO_3 from commercially available ICP multi-element standards (BDH Chemicals, Radnor, PA, USA) with concentrations ranging from 0.001 to 100 μg L^{-1}. Internal standards (ICP Internal Element Group Calibration Standard, BDH Chemicals, Radnor, PA, USA) were used to monitor signal drift for quality control. The instrument operating conditions are presented in Table S2, and the monitored isotopes are listed in Table S3. All isotopes were analyzed in collision mode with a helium and hydrogen gas mixture.

The recovery of the digestion procedure was determined by digesting and analyzing two standard reference materials for trace elements in coal fly ash: NIST SRM 1663 C (NIST, Gaithersburg, MD, USA) and BCR-176R (IRMM, Retieseweg, Geel, Belgium) [2]. For 1663 C, the recovery varied between 82% and 125% for most elements [2]. Cu exhibited high recovery of 137% and U exhibited a low recovery of 67% [2]. For BCR-176R, the recovery varied between 77% and 105% for most elements. Barium and Th exhibited low recoveries of 42% and 70%, respectively, while Zn and Se exhibited high recoveries of 131% and 146%, respectively. All elements' relative standard deviation was < 15%, indicating good precision. Samples and blanks were analyzed in triplicate.

2.3. Particle composition on single particle basis

The multi element particle composition at the single particle level was determined using SP-ICP-TOF-MS (TOFWERK, Thun, Switzerland) as performed elsewhere [3,66]. Briefly, 100 mg of the sieved ash samples were suspended in 10 mL 0.2% (by weight) FL-70 surfactant in 15 mL acid-washed centrifuge tubes, following by overhead rotation for 2 h at 40 rpm (Fisher Scientific, 88861049, USA), 60 min batch sonication with ice water (Branson 2800, 40 kHz, Danbury, CT, USA) to disperse particles, and centrifugation at 1000 g for 2 min (Eppendorf, 5810 R, Hamburg, Germany) to obtain a < 1 μm particle fraction (assuming natural particle density of 2.5 g cm^{-3}). The top 7 mL supernatant was transferred into acid-washed 15 mL centrifuge tubes. Then a surfactant, Triton X-114, and NaCl were added to the extract to achieve final concentrations of 0.2% Triton X-114 and 1 mM NaCl, respectively. The mixture was then heated at 50 °C for 1 h to form micelles. This was centrifuged at 1000 g for 5 min to create 2 phases: a surfactant-enriched phase containing the nanomaterials and water phase containing the ions. The surfactant-enriched phase containing nanomaterials was separated and stored in a refrigerator at 4 °C before SP-ICP-TOF-MS analysis. All samples were bath sonicated again for 15 min and were diluted by a factor of 100,000 prior to SP-ICP-TOF-MS analysis.

The instrument operating parameters and the monitored isotopes are summarized Tables S2 and S4, respectively. Mass spectra calibration and tuning were performed on the ICP-TOF-MS instrument daily to optimize conditions for maximum sensitivity with a multi-element tune solution (iCAP Q/RQ Tune Solution, Thermo Scientific, Ward Hill, MA, USA). Transport efficiency was calculated *via* the known size method using a certified 60-nm Au NMs (NIST RM 8013 Au, Gaithersburg, MD, USA) and a series of ionic Au standards (BDH Chemicals, West Chester, PA, USA) [50]. Dissolved calibration standards were prepared from a mixed multi-element ICP certified reference standard (0, 1, 2, 5, and 10 μg·L^{-1}, diluted in 1% HNO_3, BDH Chemicals, Radnor, PA, USA) to determine the elemental specific mass responses of particles. A 4.5% H_2/He gas mixture was used as collision gas to eliminate/minimize interferences and was optimized for $^{56}Fe^+$ and $^{28}Si^+$ signals. All samples were diluted 100,000-fold with UPW prior to analysis to avoid coincidence and eliminate dissolved background. All samples and UPW blanks were prepared and analyzed in triplicate. The SP-ICP-TOF-MS measures all isotopes (mass range of 14–275 amu) simultaneously at a sampling rate of 33 kHz. However, mass spectra were pre-averaged before readout, resulting in an integration time of 2 ms. Data were acquired for 200 s for each replicate and combined to achieve comprehensive analysis due to limited detection events of certain elements. All data processing—particle/baseline signal separation and elemental mass calculation—were performed using Tofware as described elsewhere [38,60]. The particle mass and size detection limits assuming pure metal and metal oxide phases are summarized in Table S5.

2.4. Clustering analysis of SP-ICP-TOF-MS data

The detected NMs were classified into single- and multi-metals nanomaterials (smNMs and mmNMs). The smNMs were considered as their own clusters. The mmNMs were classified into clusters of NMs of similar elemental composition using a two-stage (*e.g.,* intra- and inter-sample) agglomerative hierarchical clustering using MATLAB as described elsewhere [3,66]. First, intra-sample clustering was performed on all metal masses in each NM to generate clusters that best account for variance in NM metallic composition in each sample. This step generates a cluster dendrogram for each sample, which was divided into major clusters using a distance cutoff. A representative cluster was determined for each major cluster as the mean of metal masses in individual NMs within each cluster taking into account all elements that occurred in at least 5% of NMs within the cluster. For each major cluster, the mass fraction of a given metal in each particle was determined as the mass of that metal divided by the sum of masses of all metals in that NM.

Second, inter-sample clustering was performed on the major cluster representatives identified in the intra-sample clustering to group/cluster the similar NM major clusters identified in the different samples. This step generates a cluster dendrogram for intra-sample cluster representatives, which was divided into major clusters using a distance cutoff as performed for the intra-sample clusters. The mean intra-sample cluster composition was determined as the mean of metal mass fractions in all NMs in the cluster and was compared across samples. Selected molar elemental ratios (*e.g.,* Cr/Cu, and Cr/As) were determined on a particle-by-particle basis. The number concentration (NM g^{-1}) of the total, smNMs, mmNMs, and cluster members were determined according to SP-ICP-MS theory [51].

2.5. Transmission electron microscopy

Transmission electron microscopy (TEM) was used to study the morphology, dimensions, crystallinity, and elemental composition of NMs in ash A125. The sample was prepared for TEM analyses by the drop casting method using suspensions of WUI fire ash dispersed in methanol. The suspensions were shaken, left to sit for several minutes, and then dropped onto LC300-Cu-150 TEM grids (Electron Microscopy Sciences), which consist of a lacey C support layer attached to a 300-mesh Cu grid. TEM samples were stored in a vacuum desiccator before being analyzed. TEM data were collected at the Nanoscale Characterization and Fabrication Laboratory at Virginia Polytechnic Institute and State University on a JEOL JEM 2100 S/TEM, operated at 200 kV. TEM bright field images were acquired with a Gatan Ultrascan 1000XP CCD camera, whereas selected area electron diffraction patterns were collected with a Gatan Orius 833 slow scan CCD camera. Energy dispersive X-ray spectroscopy (EDS) elemental maps were obtained using a JEOL genuine 60 mm^2 Silicon Drift Detector.

For NM phase identification, we used a combination of compositional information from EDS analyses as well as electron diffraction data. For NMs > 200 nm, we used selected area electron diffraction, but for smaller NMs or those overlapping with adjacent material to a significant extent, we ran fast-Fourier-transforms (FFTs) on high-resolution TEM bright field images, a technique which generates diffraction patterns. Given that we used a Cu grid to hold our samples and the pole-piece in the microscope contains Cu, the distribution of Cu in EDS mapping is not necessarily inherent to the sample itself. Thus, elemental ratios from EDS analyses that include Cu (*i.e.,* Cr/Cu and Cu/As) are not a reliable means of determining possible phases on their own. As a result, we rely more on the electron diffraction measurements for determining phases.

3. Results and discussion

3.1. Total metal concentration

Among the 44 monitored elements (Table S3), only a few elements (*e.g.,* Cr, Cu, As, Fe, Al, Zn, Ti, Mn, and Ba) account for > 99% of the total elemental concentrations of all measured elements (Fig. 1). Together Cr, Cu, and As concentrations account for 28–93% of the sum of the measured elemental concentrations and 4–35% of the ash by weight. Concentrations of Cr, Cu, and As in A24 and A125 are 105–183 g Cr kg^{-1}, 72–116 g Cu kg^{-1}, and 27–44 g As kg^{-1}. These concentrations are in agreement with those measured (*e.g.,* 165 g Cr kg^{-1}, 98 g Cu kg^{-1}, and 99 g As kg^{-1}) in ashes generated by incinerating CCA-high retention level-treated wood (40 kg CCA m^{-3}) using industrial furnaces [58]. These concentrations also are much higher than those (*e.g.,* 0.11 g Cr kg^{-1}, 0.33 g Cu kg^{-1}, and 0.03 g As kg^{-1}) measured in non-treated wood ash [58]. The percent of Cr, Cu, and As concentrations in the ashes relative to the sum of Cr, Cu, and As concentrations is 51–53, 34–35%, and 13%, respectively. These percentages differ from the typical values in CCA-treated wood most commonly used for residential applications, which are 47 ± 3% Cr as CrO_3, 19 ± 2% Cu as CuO, and 34 ± 4% As as

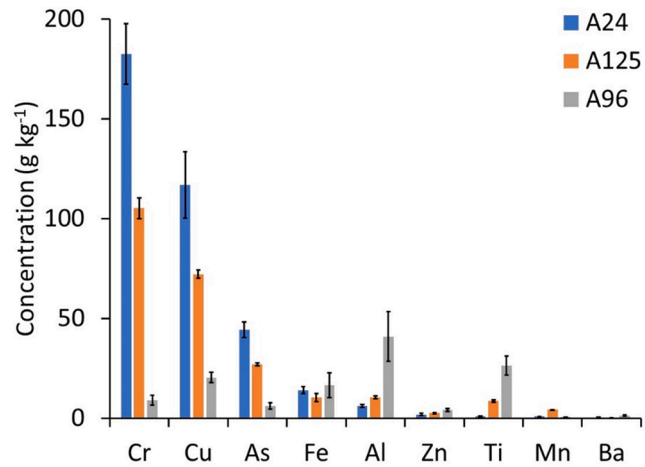

Fig. 1. Total metal concentration in the fire ashes ordered from highest element concentration to lowest concentration in A24.

As_2O_5 [15,17,48]. This is attributed to the higher volatilization of As (*e.g.,* 22–77%) compared to Cu and Cr (*e.g.,* 11–15%) to the atmosphere during the burning of CCA-treated wood. Whereas As is often considered a semi-volatile element (boiling point of 613 °C), Cr and Cu are typically considered nonvolatile (boiling points of 2672 and 2567 °C, respectively) [16]. The volatilization of As during combustion results in increased proportions of Cr and Cu relative to As in the CCA-treated wood ashes [24,27,44,67]. Elements with highest concentrations in A96 were Al (41 ± 12.4 g kg^{-1}), Ti (16.6 ± 6.3 g kg^{-1}), Cu (20.5 ± 2.6 g kg^{-1}), Fe (16.6 ± 6.3 g kg^{-1}), Cr (9.1 ± 2.4 g kg^{-1}), and As (6.1 ± 1.5 g kg^{-1}), indicating that this ash sample is derived from CCA-treated wood as well as other structural material such as sheet rock paint as well as household electronic devices. The high concentrations of Al, Ti, and Fe in A96 are consistent with the mixed gray/green color of this ash compared to the darker green color of A25 and A124. Because Cr, Cu, and As are the dominant elements in A24 and A125 and account for a substantial concentration of elements in A96, the following discussion focuses on the analysis of Cr, Cu, and As INMs by TEM and SP-ICP-TOF-MS, including elemental composition, phase, and size distributions.

3.2. Phase identification

Aggregates of Cr-, Cu-, and As-bearing INMs were identified in A125 using TEM. The aggregates range from 1510 × 1070 nm to 5850 × 3080 nm in size, but consist dominantly of smaller particles (*e.g.,* from 1370 × 820 nm to 30 × 10 nm) as shown in Fig. 2. For phase identification using TEM, we performed EDS and electron diffraction on 19 INMs present in three different aggregates and found matches to several different phases. Images, EDS maps, and electron diffraction data for three aggregates in A125 are presented in Fig. 2, S3–S7, and Table S6. Note that a bona fide phase identification for each INM phase was not always possible because the *d*-spacings of some INMs match those of multiple phases (*e.g.,* AsO_2 *vs.* As_2O_3 (monoclinic) *vs.* As_2O_3 (cubic); CrO_3 *vs.* CrO_2 *vs.* Cr_2O_3; and $CuCrO_2$ *vs.* $CuCr_2O_4$). Altogether the INMs most closely match: CrO_3, CrO_2, eskolaite (Cr_2O_3) for the Cr-bearing INMs; As_2O_5, AsO_2, claudetite (As_2O_3, monoclinic), and/or arsenolite (As_2O_3, cubic) for the As-bearing NMs; $CrAsO_4$ and $CrAs_2O_6$ for the Cr,As-bearing INMs; and $CuCrO_2$ and $CuCr_2O_4$ for the Cu,Cr-bearing NMs. An example of a Cr-, Cu-, and As-bearing INM, with its associated electron diffraction data, is shown in Fig. 2. Measurements of the *d*-spacing values of the diffraction spots of the Cr-bearing particles yielded: for the top pattern in Figure 2a—3.541, 2.945, 2.418, 2.095, and 1.451 Å, corresponding to the (−120), (200), (−2 to 20), (022), and (−3 to 40) planes of CrO_3; for the pattern in Figure 2d—4.900, 4.129,

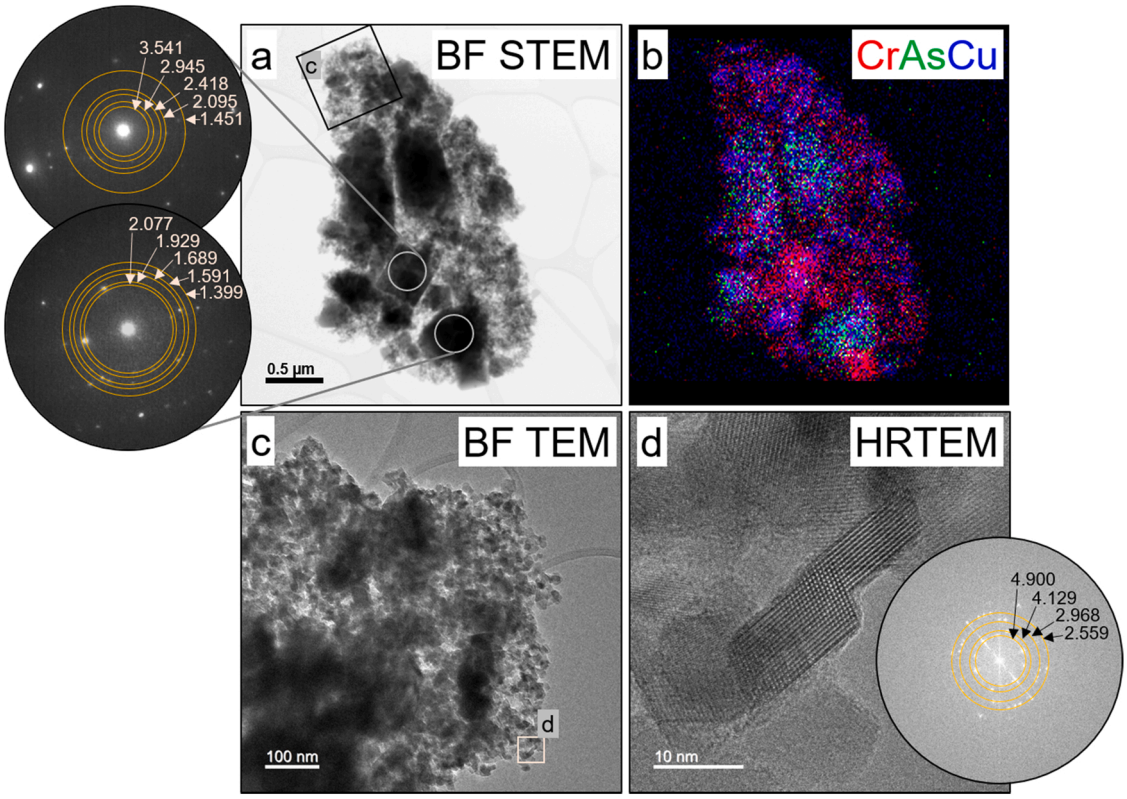

Fig. 2. Transmission electron microscopy (TEM) images, energy dispersive spectroscopy (EDS) map, and electron diffraction from Cr-, Cu-, and As-bearing nanomaterials in an aggregate from ash A125. (a) shows the aggregate's overall morphology in a bright field (BF) scanning (S)TEM image as well as two electron diffraction patterns collected from a Cr-bearing (top) and an As-bearing (bottom) particle. The *d*-spacing values of the overlaid rings are included and match the following: top pattern = CrO_3; bottom pattern = AsO_2, As_2O_3, As_2O_5, and As_4O_6. Compositional information is presented in (b) as an EDS composite X-Ray map with Cr in red, As in green, and Cu in blue. Note that the distribution of Cu is not necessarily inherent to the sample owing to the use of a Cu grid to load our sample and the fact that the polepiece in the microscope contains Cu. Higher magnification fields of view are shown in (c) as a BF TEM image and in (d) as a high resolution (HR)TEM image. (d) also includes an electron diffraction pattern extracted from the HRTEM image by performing an FFT. The *d*-spacing values of the overlaid rings are included and match CrO_3.

2.968, and 2.559 Å, corresponding to the planes (−1 to 10), (011), (200), and (03−1) of CrO_3. Measurements of the *d*-spacing values of the diffraction spots of the As-bearing particle (bottom pattern in Fig. 2a) yielded 2.077, 1.929, 1.689, 1.591, and 1.399 Å, corresponding to planes in multiple As-bearing phases (*i.e.,* AsO_2, As_2O_3 (monoclinic), As_2O_5, and As_2O_3 (cubic)) [27,46,58,67,27,46,58,67,27,46,58,67,27,46,58,67]. The identified INM phases in this study are consistent with those reported in CCA, CCA-treated wood, and CCA-treated wood ashes (Table 1) [11,24,44,57,67]. Chromated copper arsenate consists of a mixture of CrO_3, CuO, and As_2O_5 [11,15,17,48]. During the fixation of CCA reagent in wood, CrO_3 is reduced to Cr_2O_3 which then reacts with As_2O_5 to form $CrAsO_4$ [33]. However, not all As_2O_5 reacts with Cr_2O_3 during the fixation process, and some remains in the wood as unreacted reagent. Similarly, CuO remains in the treated wood as unreacted reagent [11,67]. During pyrolysis $CrAsO_4$ decomposes to Cr_2O_3 and As_2O_5 [24]. Then, As_2O_5 —unreacted and that resulting from the decomposition of $CrAsO_4$— is reduced by reductive pyrolysis vapors to As_2O_3 which starts to sublime at approximately 150–200 °C and is gasified as As_4O_6 at 330–400 °C [18, 25, 28, 33, 9]. For context, there are steep thermal gradients within wildfires; ignition of woody materials typically occurs at 250–350 °C [20,5]; soil surface temperatures reach 500–700 °C in the presence of heavy fuel [20]; and maximum flame temperatures are typically above 1000 °C [70]. In contrast, during the incineration of CCA-treated wood, CuO and Cr_2O_3 form mixed oxides, *e.g.,* $CuCrO_2$ and $CuCr_2O_4$ [39,67]. These oxides are widely synthesized by mixing CuO and Cr_2O_3 in stoichiometric amounts followed by calcination at 700–800 °C [12,35]. The dominant Cr, Cu, and As phases identified in the bottom ash of CCA-treated wood, include: $CuCrO_2$, $CuCr_2O_4$, Cr_2O_3, $MgCr_2O_4$, and $K_3Na(CrO_4)_2$ (an analogue of aphthitalite, a sulfate mineral) for Cr; $CuCrO_2$, $CuCr_2O_4$, and $Cu_3(AsO_4)_2$ for Cu; and arsenate phases with Cu and Cr as well as As_2O_3 for As [39,67].

Table 1
Speciation of Cr, Cu, and As in chromated copper arsenate (CCA)-treated wood and ashes.

	Measured CCA composition	CCA composition in treated wood	Phases identified by TEM in fire ashes
Cr	$Cr^{6+}O_3$ (47 ± 3%)	$Cr^{3+}As^{5+}O_4$	$Cr^{6+}O_3$, $Cr^{4+}O_2$, eskolaite ($Cr_2^{3+}O_3$), $Cu^{+}Cr^{3+}O_2$, $Cu^{2+}Cr_2^{3+}O_4$, $Cr^{3+}As^{5+}O_4$, $Cr^{6+}As_2^{3+}O_6$
Cu	CuO (19 ± 2%)	$Cu^{2+}O$	$Cu^{2+}Cr_2^{3+}O_4$, and $Cu^{+}Cr^{3+}O_2$
As	$As_2^{5+}O_5$ (34 ± 4%)	$As_2^{5+}O_5$, $(As^{5+}O_4)^{3-}$	$As_2^{5+}O_5$, $As^{4+}O_2$, claudetite ($As_2^{3+}O_3$, monoclinic), and arsenolite ($As_2^{3+}O_3$, cubic)
Ref	Bull[11]	Bull[11,67]	Hata et al.,[24,44,57,67]

Altogether, TEM enables probable phase identification but does not provide quantitative information on the relative abundance or number concentration of the different phases in the fire ashes. An alternative/complementary approach to TEM would be to use X-ray absorption spectroscopy to better resolve the different phases and to provide more quantitative information on the relative abundance of the different phases [67]. Additionally, SP-ICP-TOF-MS measures the masses of all elements in a single particle simultaneously, allowing the determination of INM elemental composition, size distribution, and number concentration. The former can be used to resolve the different mixed oxide

phases as discussed below. Thus, when SP-ICP-OF-MS is coupled with TEM, these techniques allow for identification of the elemental composition, size, and number concentrations of INMs.

3.3. Elemental association and ratios in single particles

Among the 37 elements monitored for SP-ICP-TOF-MS analysis (Table S5), 18 elements occurred at substantial number concentrations (*e.g.,* > 7 ×10^6 particle g^{-1}, Fig. 3a). Rare earth elements were rarely detected in the ash samples and thus were not considered for further analysis. Considering all elements, without taking into account the occurrence of NMs as mmNMs, NMs detected the most are Cr followed by Cu and As in A24, Cu and Fe in A125, and Fe and Ti in A96 (Fig. 3b). Together, Cr, Cu, and As NMs account for 40–82% of all detected NMs in the three ash samples, consistent with the contribution of these three elements (28–93%) to the sum of measured element concentrations. Chromium-bearing NMs occurred both as smNMs (22–31%) and mmNMs (69–78%, Fig. 3c). In contrast, Cu- and As-bearing NMs occurred predominantly as mmNMs (90–93% for Cu and 98% for As). Considering the occurrence of NMs as mmNMs, Cr occurs in 86%, 84%, and 52% of all NMs; Cu occurs in 63%, 67%, and 31% of all NMs; and As occurs in 11%, 7%, and 6% of all NMs in A24, A124, and A96, respectively (Fig. 3b). Together, these observations suggest that these ashes are rich in CCA constituents (Cr, Cu, and As). Nonetheless, the three ashes also contain Fe, Sb, Mn, Si, Pb, Ba, Zn, Ti, Sn, Al, Zr, V, Nb, Co, and Ni-bearing NMs (Fig. 3). A96 ash contains a significant number of Fe- and Ti-bearing NMs, accounting for 20% and 14% of all detected NMs, respectively.

Chromium-bearing NMs are associated mostly with Cu (*ca.* 51–72%), Fe and Mn (6–40%), and As (8–12%) (Fig. 4a). Copper-bearing NMs are associated mainly with Cr (85–92%), Fe (7–47%), Mn (8–44%), and As (10–17%) (Fig. 4b). Arsenic-bearing NMs are associated with Cr (98%), Cu (92–97%), Mn (27–79%), and Pb (24–73%) (Fig. 4c). These associations between Cr, Cu, and As indicate that they form mmNMs, in agreement with the phases identified by TEM as well as with previous studies demonstrating that Cr and Cu occur dominantly in the mixed oxide phases, *e.g.,* $CuCrO_2$ and $CuCr_2O_4$ [67].

The molar ratios of Cr/Cu, Cr/As, and Cu/As in all CrCu, CrAs, and CuAs-bearing mmNMs are presented in Fig. 5. The molar ratio Cr/Cu show a broad distribution between 0.003 and 220, with median ratios of 1.0–2.0 and most ratios (*e.g.,* 72–88%) between 0 and 3. These ratios can be attributed to $CuCrO_2$ and $CuCr_2O_4$, whereas higher ratios can be ascribed to aggregates of these phases with Cr-smNMs. The molar ratios of Cr/As and Cu/As exhibit broad distributions between 0.2 and 120 and 0.1 and 240, with median ratios of 2.5 and 1.3, respectively. The low values of Cr/As can be ascribed to phases such as $CrAsO_4$ and $CrAs_2O_6$. The higher ratios can be ascribed to the aggregation of Cr-, Cu-, and As-bearing smNMs and mmNMs, as well as and the volatilization of As

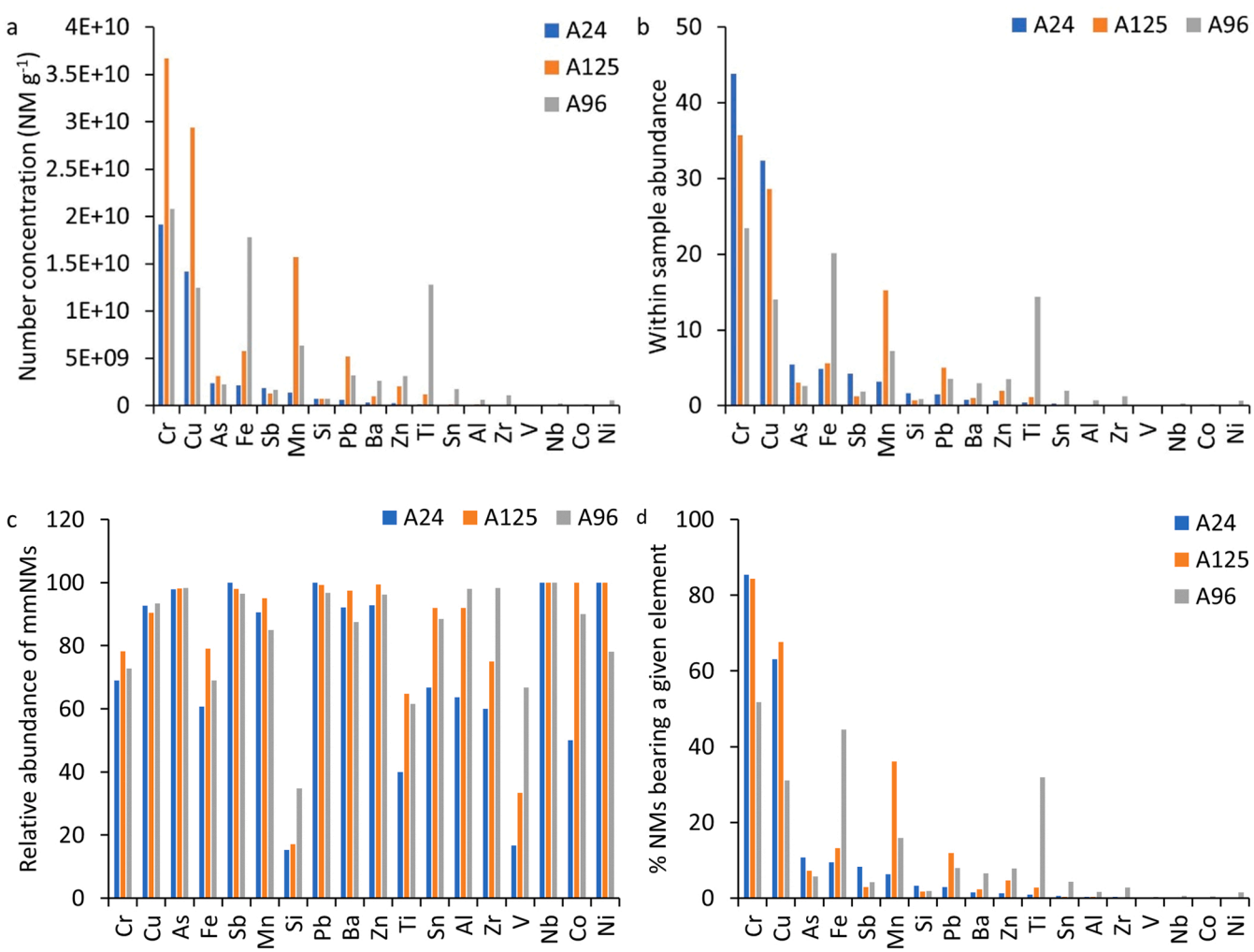

Fig. 3. Characterization of ash samples by single particle-inductively coupled plasma-time of flight-mass spectrometry (SP-ICP-TF-MS): (a) number concentration of the detected nanomaterials (NMs), (b) within sample relative abundance of the metal-bearing NMs considering all signals as single-element single particles, (c) relative abundance (%) of multi-metal nanomaterials (mmNMs) for each element, and (d) % of particles containing a given element.

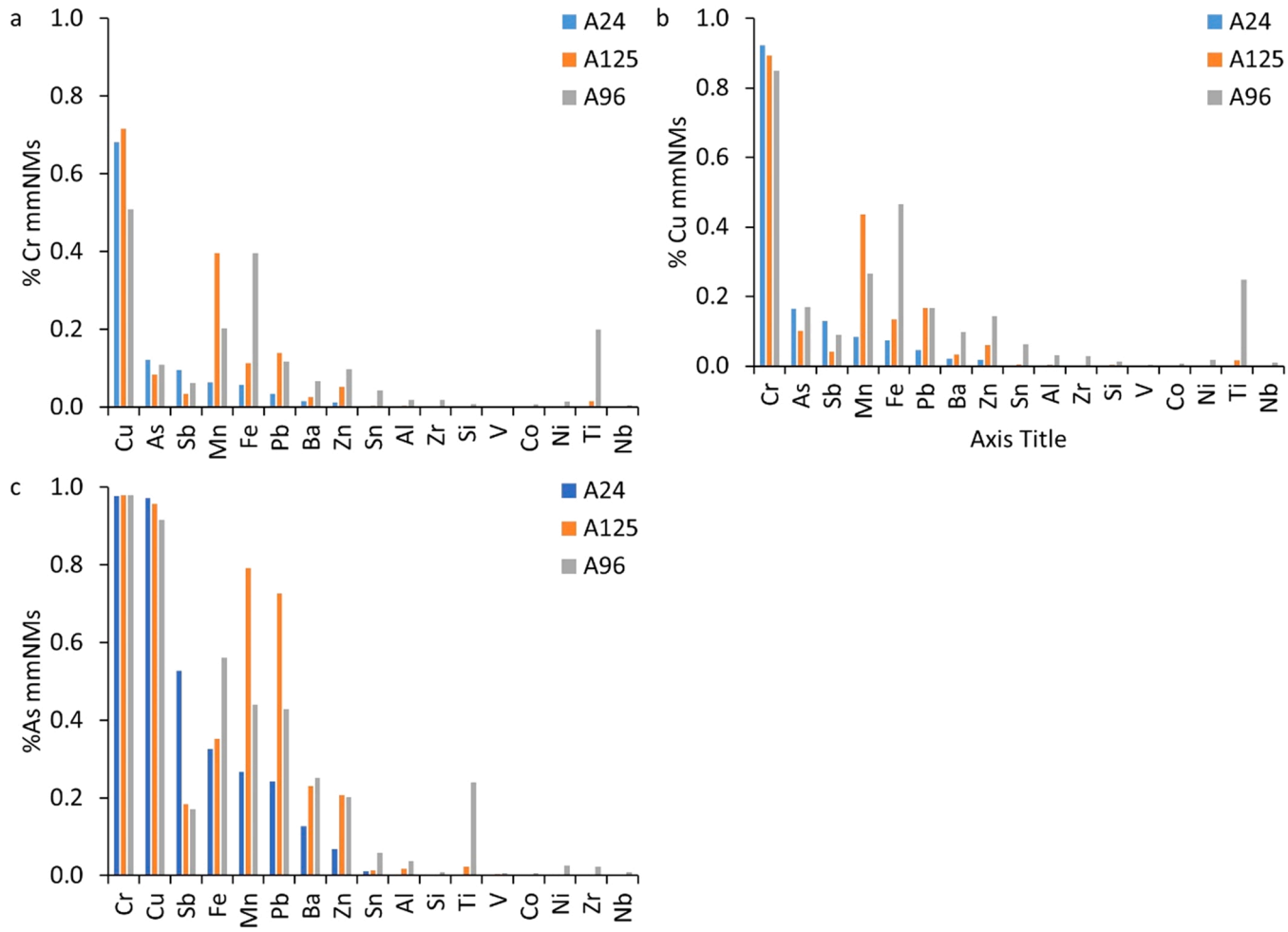

Fig. 4. Association of (a) Cr, (b) Cu, and (c) As with other elements in multi-metal nanomaterials (mmNMs)s extracted from the fire ashes.

during the combustion of CCA-treated wood. These findings are consistent with the Cr-, Cu-, and As-phases identified by TEM.

3.4. Clusters of NMs

Eight major compositional clusters of NMs were identified in A24 and A125, and 13 in A96 (Fig. S8a). They include Cr, Cu, Ni, Al, Fe, Mn, Ti, Zn, Si, Sn, Sb, Ba, and Zr-rich particle clusters. Chromium, Cu, and As occur as major elements in some clusters but are also scattered as minor constituents in other clusters, such as Al-, Si-, Fe-rich mmNM clusters. The occurrence of Cr, Cu, and As as a minor phase in Al-, Si-, and Fe-rich mmNM clusters is due to the heteroaggregation of Cr, Cu, and As-bearing mmNMs with other mmNMs, such as Al, Si, Fe, and Ti. This is the case particularly for A96, which is characterized by light green/gray color, whereas A24 and A125 are characterized by darker green colors (Fig. S2), indicating the higher contribution of CCA byproducts in A24 and A125. This is also consistent with the total elemental concentrations, which show that Cr, Cu, and As account for 93% in A24 and 83% in A125 of the total masses of measured elements. In contrast, Cr, Cu, and As account for only 24% of the total measured element masses in A96. The second stage clustering generated 14 major clusters (Fig. S8b and S9), including Si, Ti, Ba, Fe, Ni, Sb, Al, Sn, Cr, As, Cu, Mn, and Zn-rich particle clusters. The CrCuFe cluster accounts for 97% of mmNMs in A24 and A125 and 47% in A96 (Fig. S10). The TiFeCr cluster accounts for 32% of mmNMs in A96 and $< 2\%$ in A24 and A125. The FeNiCr cluster accounts for 12% of mmNMs in A96 and $< 1\%$ in A24 and A125. The CuFeCr accounts for 3.4% in A96, 0.64% in A24, and 0% in A125.

The Cr/Cu and Cr/As molar ratios in the Cr, Cu, and As-bearing mmNM clusters are presented in Fig. S11. The molar Cr/Cu ratio in the CrCuFe cluster ranges from 0.25 to 332 with a peak Cr/Cu of 1.0 (Fig. S11a). The molar Cr/As ratio in the CrCuFe cluster ranges from 1 to 1000 with a peak centered at 4.0 (Fig. S11b). Based on these ratios, this cluster contains a mixture of $CrCuO_2$, $CuCr_2O_4$, and aggregates of Cr, Cu, and As-smNMs and mmNMs. The molar Cr/Cu ratio in the CuFeCr cluster ranges from 0.2 to 1.4 (Fig. S11c) and is most likely attributed to $CrCuO_2$ mmNMs forming heteroaggregates with Fe-bearing NMs. The Cr/As ratio in the AsCrCu cluster ranges from 0.4 to 3.0 (Fig. S11d) and thus is ascribed to $CrAsO_4$.

To further understand the Cr, Cu, As associations within mmNMs, the two-stage clustering analysis was performed again on Cr, Cu, and As bearing mmNMs only. Seven clusters, including three CrCuAs, one CuCrAs, one CrAsCu, one AsCrCu, and one AsCu were identified (Fig. 6a). The mean mass fractions of mmNMs in each cluster, the number concentration of mmNMs in each cluster of the identified mmNM clusters are presented in Fig. 6, and the probable phase for each cluster is presented in Table 2. Three clusters, including two CrCuAs with different elemental compositions and a CuCrAs clusters (cluster 1–3 in Table 2) account for $> 95\%$ of Cr, Cu, and As INMs in the three ashes. Based on the Cr/Cu molar elemental ratios (Table 2), the first cluster is ascribed to aggregates of Cr, Cu, and As-bearing smNMs and mmNMs and accounts for 38–73% of all Cr, Cu, and As mmNMs in the three ashes. The second cluster is ascribed to a mixture of $CuCrO_4$ and $CuCr_2O_4$ and accounts for 25–49% of all Cr, Cu, and As mmNMs in the three ashes. The third cluster is also ascribed to $CuCrO_2$ and accounts for 2–9% of all mmNMs. It is worth noting that the extensive aggregation of Cr, Cu, and As smNMs and mmNMs illustrated by TEM hampered the

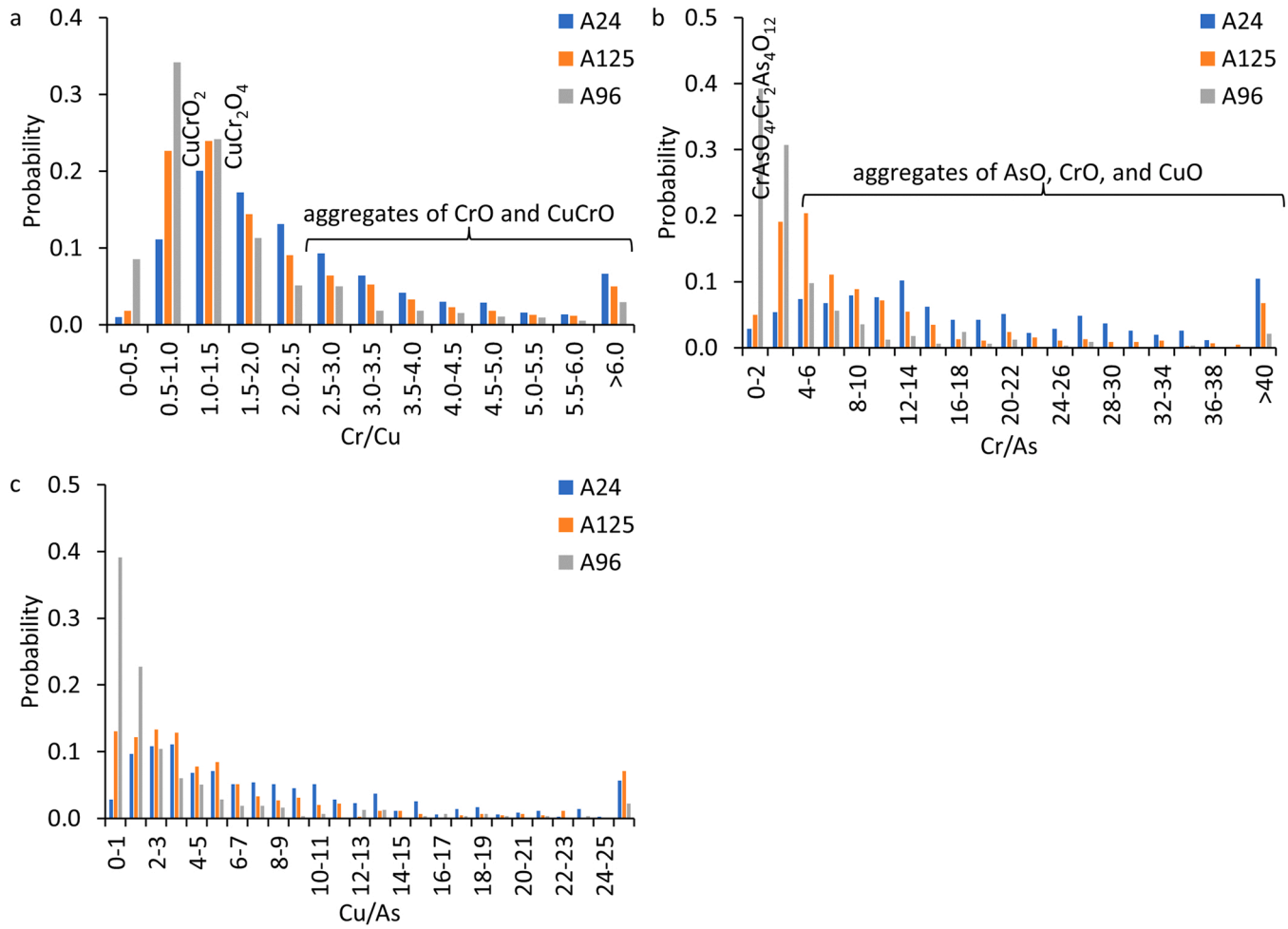

Fig. 5. Molar ratios of (a) Cr/Cu, (b) Cr/As, and (c) Cu/As in all Cr and Cu-bearing multi-metal nanomaterials (mmNMs), Cr and As-bearing mmNMs, and Cu and As-bearing mmNMs, respectively.

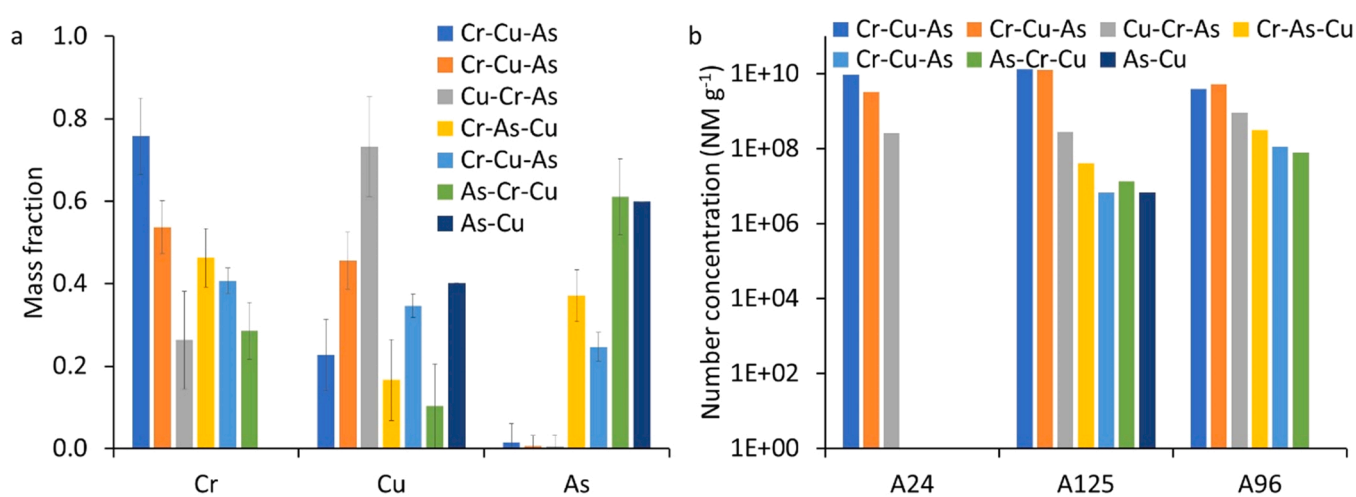

Fig. 6. (a) Elemental composition (*e.g.,* mean mass fraction) and (b) number concentration of CrCuAs multi-metal nanomaterials (mmNM) clusters. Two stage hierarchical clustering was performed on Cr, Cu, and As bearing particles only with first and second stage cutoffs of 0.05 and 0.2. The error bars in panel a represent the standard deviation of the mass fractions of the individual particles measured by SP-ICP-TOF-MS.

categorical classification of mmNMs (*e.g.,* $CuCrO_4$ *vs.* $CuCr_2O_4$). Such a limitation could be overcome by further breaking down aggregates into their primary forming particles. Overall, these findings are consistent with previous studies demonstrating that Cu and Cr present in CCA-treated wood ash coexist predominantly in the two oxide phases: $CuCr_2O_4$ and $CuCrO_2$ [67]. The differences in the abundance of $CuCr_2O_4$ and $CuCrO_2$ in the fire ash might be attributed to differences in the fire conditions, such as fire temperature and duration. Chemical equilibrium

Table 2
Molar elemental ratios in Cr, Cu, and As bearing multi-metal nanomaterials (mmNM) clusters and the probable phases in each cluster.

Cluster #	Cluster	Median Cr/Cu	Median Cr/As	Relative abundance	Probable phase
1	CrCuAs	2.1–17.2	3.7–38.0	73% in A24 50% in A125 38% in A96	Aggregates of Cr, Cu, and As smNMs and mmNMs
2	CrCuAs	1.3–1.6	8.5–33.5	25% in A24 49% in A125 49% in A96	$CuCrO_2$ + As-phases
3	CuCrAs	0.2–0.8	1.4–20.1	2% in A24 1.1% in A125 8.6% in A96	Aggregate of smNMs
4	CrAsCu	1.8–5.7	1.35–2.2	0.15% in A125 3% in A96	$Cr_2As_4O_{12}$
5	CrCuAs	1.2–1.5	2.4–2.7	0.03% in A125 1.0% in A96	$CuCrO_2$ + As-phases
6	AsCrCu	1.22–3.54	0.7–0.8	0.5% in A125 0.7% in A96	$CrAsO_4$
7	AsCu			0.03% in A125	

model calculations demonstrate that, in the residual ash, Cu forms $CuCr_2O_4$ at low to medium temperatures (*e.g.,* 400–900 °C), $CuCrO_2$ at high temperatures (*e.g.,* > 900 °C), and minor amounts of CuO at medium temperatures (*e.g.,* 700–900 °C) [39]. Besides copper chromium oxides, Cr also forms Cr_2O_3 at high temperatures (> 900 °C). However, experimental combustion of CCA-treated wood demonstrated the occurrence of mixtures of the different Cr, Cu, and As phases at low and high temperatures due to local temperature variations during the combustion process; this is likely owing to the fact that actual particle burning temperatures are significantly higher than the measured furnace temperatures [39].

The particle size distributions of all Cr-, Cu-, and As-bearing NMs are presented in Fig. 7, assuming single element compositions and one phase of Cr_2O_3, CuO, and As_2O_3. These size distributions cover a broad range of sizes of 60–1000 nm, with 15–52% of Cr-bearing NMs, 44–55% of Cu-bearing NMs, and < 4% As-bearing NMs within the nano-size range (*e.g.,* < 100 nm). These sizes are in general agreement with the aggregate sizes, but much larger than the primary NM sizes as measured by TEM. A96 contains a higher fraction of particles < 100 nm (*e.g.,* 52% of Cr, 55% of Cu, and 4% of As) than A24 and A125 (15–17% of Cr, 44% of Cu, and 0–0.3% of As). These differences in mmNM sizes might be attributed to differences in fire conditions.

4. Conclusions and environmental implications

This study presents a comprehensive characterization of three wildland-urban interface (WUI) fire ash samples collected from burned

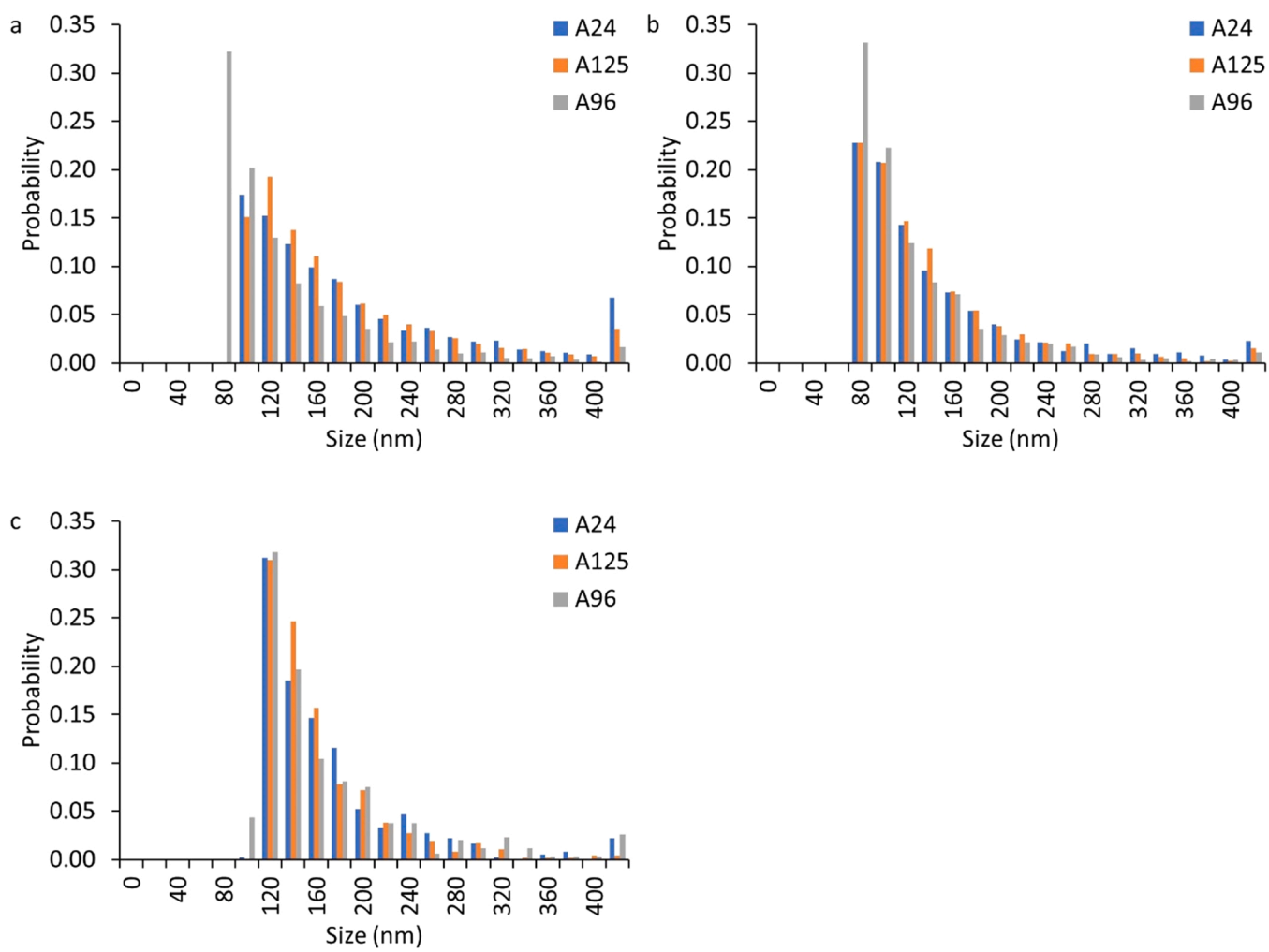

Fig. 7. Particle size distribution of (a) Cr, (b) Cu, and (c) As-bearing nanomaterials (NMs).

residential structures following the 2020 LNU Lightening Complex fire in California and suspected to be derived from the combustion of chromated copper arsenate (CCA)-treated wood, using state-of-the-art analytical methodologies, including TEM and SP-ICP-TOF-MS. Together, Cr, Cu, and As concentrations account for 24%, 83%, and 93% of the total mass of measured elements in the three ashes, consistent with origin from CCA-treated wood. The authors are not aware of any previous detailed studies of ash derived from CCA-treated wood in a field setting. TEM analyses indicate that Cr, Cu, and As occur as heteroaggregates of single-metal and multi-metal nanomaterials (smNM and mmNM) with potential matches to the following phases: CrO_3, CrO_2, eskolaite (Cr_2O_3), $CuCrO_2$, $CuCr_2O_4$, $CrAsO_4$, $CrAs_2O_6$, As_2O_5, AsO_2, claudetite (As_2O_3. monoclinic), and/or arsenolite (As_2O_3, cubic). SP-ICP-TOF-MS analyses reveal that Cr occurs as a mixture of smNM and mmNM containing Cr, Cu, and As; Cu occurs predominantly as mmNM containing Cr and As; and As occurs exclusively as mmNM containing Cr and Cu. Hierarchical clustering analyses uncover several Cr, Cu, and As clusters. The molar ratios of Cr/Cu and Cr/As within these clusters are consistent with the phases identified by TEM as well as their heteroaggregates, in particular $CuCrO_2$, $CuCr_2O_4$, and $CrAsO_4$. These mmNM clusters account for the majority of the number of Cr, Cu, and As mmNMs. Thus, this study demonstrates that WUI fires transform CCA initial constituents (CrO_3, CuO, and As_2O_5) into new INM phases (*e.g.,* $CuCrO_2$, $CuCr_2O_4$, and $CrAsO_4$) and result in their release into the surrounding environment, where they may pose human health risks. For instance, Peters et al. [53,54] report on a clinical case of As poisoning of a family living in rural Wisconsin who had used CCA-treated plywood as a source of fuel for their woodstove [53,54]. The environmental risks of fire ashes are not well characterized, and include release, transport and exposure to transformed metal phases of variable bioavailability. This study also provides a comprehensive approach for the characterization of CCA-treated wood ashes and for tracking CCA constituents in environmental systems based on multi-element analysis using SP-ICP-TOF-MS.

Ash, and its associated contaminants, present health risks to people (*e.g.,* fire recovery workers, residents) and communities through direct and indirect ingestion, inhalation, and absorption. People are likely exposed to INMs in the fire ashes through disturbance and resuspension of the ashes (*e.g.,* from walking, cleaning, wind), which may be inhaled [1]. Additionally, wind transfers ashes from one location to another, and rainfall generates runoff that transports ashes and associated NMs into surrounding soils and surface water bodies, where they may pose potential threats to environmental and human health. Health effects of ash exposure range from acute symptoms, such as coughing, sneezing, and throat and eye irritation, to chronic disease and increased cancer risk [22,65]. Additionally, ashes of CCA-treated wood could be more toxic than those of untreated wood. For instance, both untreated and CCA-treated wood ash presented a carcinogenic risk for the same cell line (A549), with higher effects of CCA-treated wood ash [19,49].

Furthermore, several studies demonstrated the potential release of Cr, Cu, and As from CCA-treated wood and the subsequent environmental and human health effects — such as neurotoxicity, carcinogenicity, and cell pathophysiology — mainly due to the toxic effects of As, Cu, and/or Cr [34,43,40,41,42,49,59]. The risk could be even higher when treated wood is burned likely due to transformation of CCA constituents (CrO_3, CuO, and As_2O_5) into new INM phases (*e.g.,* $CuCrO_2$, $CuCr_2O_4$, and $CrAsO_4$) which might possess higher reactivity, bioavailability and/or toxicity compared to the initial CCA constituents. For instance, some of the identified INMs (*e.g.,* $CuCrO_2$ and $CuCr_2O_4$) possess (photo)-catalytic properties [32,55,71] and may play important roles in catalyzing reactions in the environment and in organisms, such as the degradation of organic matter and the decomposition of hydrogen peroxide leading to the formation of reactive oxygen species, which in turn induce oxidative stress, a well-known disease mechanism [21]. Other identified INMs (*e.g.,* CuO, CrO_3, CrO_2, and Cr_2O_3) also could pose risks to environmental and human health as discussed elsewhere [36, 61].

Environmental Implication

This study reports the concentrations and nature of Cr, Cu, and As-bearing incidental nanomaterials (INMs) in WUI fire ashes collected from residential structures. The studied ashes contain mainly heteroaggregates of single and multi-element Cr, Cu, and As-bearing INMs, including CrO3, CrO2, eskolaite (Cr2O3), CuCrO2, CuCr2O4, CrAs2O6, As2O5, AsO2, claudetite (As2O3, monoclinic), or arsenolite (As2O3, cubic), consistent with phases identified in CCA-treated wood ashes. Thus, WUI fires can lead to significant release of a mixture of the initial CCA constituents and their transformed byproducts in the form of INMs, which may pose increased risks to environmental and human health.

CRediT authorship contribution statement

Mr. Mahbub Alam performed single particle analysis. Mr. Talal Alshehri performed ash digestion and total metal concentration analysis. Dr. Mohammed Baalousha conceived the overall idea of the research, coordinated the collaboration among the research team, supervised Mr. Mahbub Alam and Mr. Talal Alshehri in performing experimental work and data analysis, and write the first draft. Dr. Charles N. Alpers performed field sampling campaigns and provided background information on the sampling sites and the collected samples. Dr. Sheryl A. Singerling performed transmission electron microscopy analysis and the associated data analysis. All authors contributed to the manuscript writing and editing.

Declaration of Competing Interest

The authors declare that they have no known competing financial interests or personal relationships that could have appeared to influence the work reported in this paper.

Data Availability

Data will be made available on request.

Acknowledgments

This work was supported by a RAPID grant (2101983) from the National Science Foundation (NSF), by the Nanoscale Characterization and Fabrication Laboratory and the Virginia Tech National Center for Earth and Environmental Nanotechnology Infrastructure (NanoEarth), a member of the National Nanotechnology Coordinated Infrastructure (NNCI), supported by NSF (ECCS 1542100 and ECCS 2025151), and by the U.S. Geological Survey (USGS) Toxic Substances Hydrology Program, Minerals Integrated Science Team, under the Environmental Health Program of the USGS Ecosystem Mission Area. Any use of trade, firm, or product names is for descriptive purposes only and does not imply endorsement by the U.S. Government.

Appendix A. Supporting information

Supplementary data associated with this article can be found in the online version at doi:10.1016/j.jhazmat.2022.130608.

References

[1] Alexakis, D.E., 2020. Suburban areas in flames: Dispersion of potentially toxic elements from burned vegetation and buildings. Estimation of the associated ecological and human health risk. Environ Res 183, 109153. https://doi.org/10.1016/j.envres.2020.109153.

[2] T. Alshehri , J. Wang , S.A. Singerling , J. Gigault , J.P. Webster , S.J. Matiasek , et al. , Wildland-urban interface fire ashes as a major source of incidental nanomaterials. Journal of Hazardous Materials (In Press) (2022).

[3] Baalousha, M., Wang, J., Erfani, M., Goharian, E., 2021. Elemental fingerprints in natural nanomaterials determined using SP-ICP-TOF-MS and clustering analysis. Sci Total Environ 792, 148426. https://doi.org/10.1016/j.scitotenv.2021.148426.

[4] Baalousha, M., Desmau, M., Singerling, S., Webster, J.P., Matiasek, S., Stern, M.A., et al., 2022. Discovery and potential ramifications of reduced iron-bearing nanomaterials—magnetite, wüstite, and zero valent iron—in wildland-urban interface fire ashes. Environ Sci Nano.

[5] Babrauskas, V., 2002. Ignition of wood: a review of the state of the art. J Fire Prot Eng 12 (3), 163–189.

[6] Barton, C., 2014. CCA-Treated Wood. In: Wexler, P. (Ed.), Encyclopedia of Toxicology, Third ed. Academic Press, Oxford, pp. 751–752. https://doi.org/10.1016/B978-0-12-386454-3.00272-4.

[7] Bixby, R.J., Cooper, S.D., Gresswell, R.E., Brown, L.E., Dahm, C.N., Dwire, K.A., 2015. Fire effects on aquatic ecosystems: an assessment of the current state of the science. Freshw Sci 34 (4), 1340–1350.

[8] Bladon, K.D., Emelko, M.B., Silins, U., Stone, M., 2014. Wildfire and the Future of Water Supply. Environ Sci Technol 48 (16), 8936–8943. https://doi.org/10.1021/es500130g.

[9] Bridgwater, A.V., 2008. Progress in Thermochemical Biomass Conversion. John Wiley & Sons.

[10] Brito, D.Q., Passos, C.J.S., Muniz, D.H., Oliveira-Filho, E.C., 2017. Aquatic ecotoxicity of ashes from Brazilian savanna wildfires. Environ Sci Pollut Res 24 (24), 19671–19682.

[11] Bull, D.C., 2001. The chemistry of chromated copper arsenate II. Preservative-wood interactions. Wood Sci Technol 34 (6), 459–466. https://doi.org/10.1007/s002260000066.

[12] Campos, E.A., Dutra, R.D.C.L., Rezende, L.C., Diniz, M.F., Nawa, W.M.D., Iha, K., 2010. Performance evaluation of commercial copper chromites as burning rate catalyst for solid propellants. J Aerosp Technol Manag 2, 323–330.

[13] Campos, I., Abrantes, N., 2021. Forest fires as drivers of contamination of polycyclic aromatic hydrocarbons to the terrestrial and aquatic ecosystems. Curr Opin Environ Sci Health 24, 100293. https://doi.org/10.1016/j.coesh.2021.100293.

[14] Campos, I., Abrantes, N., Keizer, J.J., Vale, C., Pereira, P., 2016. Major and trace elements in soils and ashes of eucalypt and pine forest plantations in Portugal following a wildfire. Sci Total Environ 572, 1363–1376.

[15] Chen, A.Y.-Y., Olsen, T., 2016. Chromated copper arsenate–treated wood: a potential source of arsenic exposure and toxicity in dermatology. Int J Women's Dermatol 2 (1), 28–30.

[16] L.B. Clarke, L.L. Sloss, Trace elements-emissions from coal combustion and gasification. (1992).

[17] Coles, C.A., Arisi, J.A., Organ, M., Veinott, G.I., 2014. Leaching of chromium, copper, and arsenic from CCA-treated utility poles. Appl Environ Soil Sci 2014.

[18] Cuypers, F., De Dobbelaere, C., Hardy, A., Van Bael, M.K., Helsen, L., 2009. Thermal behaviour of arsenic trioxide adsorbed on activated carbon. J Hazard Mater 166 (2–3), 1238–1243.

[19] Danielsen, P.H., Loft, S., Kocbach, A., Schwarze, P.E., Møller, P., 2009. Oxidative damage to DNA and repair induced by Norwegian wood smoke particles in human A549 and THP-1 cell lines. Mutat Res /Genet Toxicol Environ Mutagen 674 (1), 116–122. https://doi.org/10.1016/j.mrgentox.2008.10.014.

[20] DeBano, L.F., Neary, D.G., Ffolliott, P.F., 1998. Fire Effects on Ecosystems. John Wiley & Sons.

[21] Forrester, S.J., Kikuchi, D.S., Hernandes, M.S., Xu, Q., Griendling, K.K., 2018. Reactive oxygen species in metabolic and inflammatory signaling. Circ Res 122 (6), 877–902.

[22] Groot, E., Caturay, A., Khan, Y., Copes, R., 2019. A systematic review of the health impacts of occupational exposure to wildland fires. Int J Occup Med Environ Health 32 (2), 121–140.

[23] Harper, A.R., Santin, C., Doerr, S.H., Froyd, C.A., Albini, D., Otero, X.L., et al., 2019. Chemical composition of wildfire ash produced in contrasting ecosystems and its toxicity to Daphnia magna. Int J Wildland Fire 28 (10), 726–737. https://doi.org/10.1071/WF18200.

[24] Hata, T., Bronsveld, P.M., Vystavel, T., Kooi, B.J., De Hosson, J.T.M., Kakitani, T., et al., 2003. Electron microscopic study on pyrolysis of CCA (chromium, copper and arsenic oxide)-treated wood. J Anal Appl Pyrolysis 69, 635–643. https://doi.org/10.1016/S0165-2370(03)00077-9.

[25] Helsen, L., Van den Bulck, E., 2003. Metal retention in the solid residue after low-temperature pyrolysis of chromated copper arsenate (CCA)-treated wood. Environ Eng Sci 20 (6), 569–580.

[26] Helsen, L., Van den Bulck, E., 2005. Review of disposal technologies for chromated copper arsenate (CCA) treated wood waste, with detailed analyses of thermochemical conversion processes. Environ Pollut 134 (2), 301–314.

[27] Helsen, L., Van den Bulck, E., Mullens, S., Mullens, J., 1999. Low-temperature pyrolysis of CCA-treated wood: thermogravimetric analysis. J Anal Appl Pyrolysis 52 (1), 65–86. https://doi.org/10.1016/S0165-2370(99)00034-0.

[28] Helsen, L., Van den Bulck, E., Van Bael, M., Mullens, J., 2003. Arsenic release during pyrolysis of CCA treated wood waste: current state of knowledge. J Anal Appl Pyrolysis 68, 613–633.

[29] Heringa, M., Peters, R., Bleys, R., Van Der Lee, M., Tromp, P., Van Kesteren, P., et al., 2018. Detection of titanium particles in human liver and spleen and possible health implications. Part Fibre Toxicol 15 (1), 1–9.

[30] Hoover, K., Hanson, L.A., 2021. Wildfire statistics. Congr Res Serv 2.

[31] Jambeck, J., Weitz, K., Solo-Gabriele, H., Townsend, T., Thorneloe, S., 2007. CCA-Treated wood disposed in landfills and life-cycle trade-offs with waste-to-energy and MSW landfill disposal. Waste Manag 27 (8), S21–S28.

[32] de Jesus Cubas, P., Semkiw, A.W., Monteiro, F.C., Los Weinert, P., Monteiro, J.F.H. L., Fujiwara, S.T., 2020. Synthesis of CuCr2O4 by self-combustion method and photocatalytic activity in the degradation of Azo Dye with visible light. J. Photochem Photobiol A Chem 401, 112797.

[33] Kakitani, T., Hata, T., Kajimoto, T., Imamura, Y., 2004. Two possible pathways for the release of arsenic during pyrolysis of chromated copper arsenate (CCA)-treated wood. J Hazard Mater 113 (1-3) 247–252.

[34] Katz, S.A., Salem, H., 2005. Chemistry and toxicology of building timbers pressure-treated with chromated copper arsenate: a review. J Appl Toxicol Int J 25 (1), 1–7.

[35] Kawamoto, A.M., Pardini, L.C., Rezende, L.C., 2004. Synthesis of copper chromite catalyst. Aerosp Sci Technol 8 (7), 591–598.

[36] Lead, J.R., Batley, G.E., Alvarez, P.J., Croteau, M.N., Handy, R.D., McLaughlin, M. J., et al., 2018. Nanomaterials in the environment: behavior, fate, bioavailability, and effects—an updated review. Environ Toxicol Chem 37 (8), 2029–2063.

[37] Lee, S., Bi, X., Reed, R.B., Ranville, J.F., Herckes, P., Westerhoff, P., 2014. Nanoparticle Size Detection Limits by Single Particle ICP-MS for 40 Elements. Environ Sci Technol 48 (17), 10291–10300.

[38] Loosli, F., Wang, J., Rothenberg, S., Bizimis, M., Winkler, C., Borovinskaya, O., et al., 2019. Sewage spills are a major source of titanium dioxide engineered (nano)-particle release into the environment. Environ Sci Nano 6 (3), 763–777.

[39] Lundholm, K., Rogers, J.M., Haynes, B.S., Boström, D., Nordin, A., 2008. Fate of Cu, Cr, and As during the Combustion Stages of CCA-Treated Wood Fuel Particles. Energy Fuels 22 (3), 1589–1597. https://doi.org/10.1021/ef700621y.

[40] Matos, R.C., Vieira, C., Morais, S., de Lourdes Pereira, M., de Jesus, J.P., 2009. Nephrotoxicity of CCA-treated wood: a comparative study with As2O5 and CrO3 on mice. Environ Toxicol Pharmacol 27 (2), 259–263. https://doi.org/10.1016/j.etap.2008.11.009.

[41] Matos, R.C., Vieira, C., Morais, S., Pereira, M.D.L., Pedrosa, J., 2009. Nephrotoxicity effects of the wood preservative chromium copper arsenate on mice: Histopathological and quantitative approaches. J Trace Elem Med Biol 23 (3), 224–230. https://doi.org/10.1016/j.jtemb.2009.03.008.

[42] Matos, R.C., Vieira, C., Morais, S., Pereira, M.L., Pedrosa, J., 2010. Toxicity of chromated copper arsenate: a study in mice. Environ Res 110 (5), 424–427. https://doi.org/10.1016/j.envres.2010.03.001.

[43] Matos, R.C., Oliveira, H., Fonseca, H.M.A.C., Morais, S., Sharma, B., Santos, C., et al., 2020. Comparative Cr, As and CCA induced cytostaticity in mice kidney: a contribution to assess CCA toxicity. Environ Toxicol Pharmacol 73, 103297. https://doi.org/10.1016/j.etap.2019.103297.

[44] McMahon, C.K., Bush, P.B., Woolson, E.A., 1986. How much arsenic is released when CCA wood is burned? For. Prod. J. 36 (11/12), 45–50.

[45] de Medeiros Domingos, D., Scussel, R., Canever, S.B., Soares, B.Q., Angioletto, E., Bernardin, A.M., et al., 2022. Toxicity of fly ash effluent from the combustion of (chromated copper arsenate)-treated wood. Clean. Mater. 3, 100051.

[46] Miller, J.D., Safford, H., Crimmins, M., Thode, A.E., 2009. Quantitative evidence for increasing forest fire severity in the Sierra Nevada and southern Cascade Mountains, California and Nevada, USA. Ecosystems 12 (1), 16–32.

[47] Montaño, M.D., Olesik, J.W., Barber, A.G., Challis, K., Ranville, J.F., 2016. Single particle ICP-MS: advances toward routine analysis of nanomaterials. Anal Bioanal Chem 408 (19), 5053–5074.

[48] Morais, S., Fonseca, H.M., Oliveira, S.M., Oliveira, H., Gupta, V.K., Sharma, B., et al., 2021. Environmental and health hazards of chromated copper arsenate-treated wood: a review. Int J Environ Res Public Health 18 (11), 5518.

[49] Ohgami, N., Yamanoshita, O., Thang, N.D., Yajima, I., Nakano, C., Wenting, W., et al., 2015. Carcinogenic risk of chromium, copper and arsenic in CCA-treated wood. Environ Pollut 206, 456–460. https://doi.org/10.1016/j.envpol.2015.07.041.

[50] Pace, H.E., Rogers, N.J., Jarolimek, C., Coleman, V.A., Higgins, C.P., Ranville, J.F., 2011. Determining transport efficiency for the purpose of counting and sizing nanoparticles via single particle inductively coupled plasma mass spectrometry. Anal Chem 83 (24), 9361–9369.

[51] Pace, H.E., Rogers, N.J., Jarolimek, C., Coleman, V.A., Gray, E.P., Higgins, C.P., et al., 2012. Single particle inductively coupled plasma-mass spectrometry: a performance evaluation and method comparison in the determination of nanoparticle size. Environ Sci Technol 46 (22), 12272–12280.

[52] Pedersen, A.J., Ottosen, L.M., 2006. Elemental analysis of ash residue from combustion of CCA treated wood waste before and after electrodialytic extraction. Chemosphere 65 (1), 110–116. https://doi.org/10.1016/j.chemosphere.2006.02.021.

[53] Peters, H.A., Croft, W.A., Woolson, E.A., Darcey, B.A., Olson, M.A., 1983. Arsenic, chromium, and copper poisoning from burning treated wood. N Engl J Med 308 (22), 1360–1361.

[54] Peters, H.A., Croft, W.A., Woolson, E.A., Darcey, B.A., Olson, M.A., 1984. Seasonal arsenic exposure from burning chromium-copper-arsenate-treated wood. JAMA 251 (18), 2393–2396.

[55] Prasad, R., Singh, P., 2011. Applications and preparation methods of copper chromite catalysts: a review. Bull Chem React Eng Catal 6 (2), 63–113.

[56] Radeloff, V.C., Helmers, D.P., Kramer, H.A., Mockrin, M.H., Alexandre, P.M., Bar-Massada, A., et al., 2018. Rapid growth of the US wildland-urban interface raises wildfire risk. Proc Natl Acad Sci 115 (13), 3314–3319.

[57] Sandelin, K., Backman, R., 2000. Equilibrium distribution of arsenic, chromium, and copper when burning impregnated wood. Combustion and Materials Chemistry. Abo Akademi Process Chemistry Group, pp. 0–8.

[58] Solo-Gabriele, H.M., Townsend, T.G., Messick, B., Calitu, V., 2002. Characteristics of chromated copper arsenate-treated wood ash. J Hazard Mater 89 (2), 213–232. https://doi.org/10.1016/S0304-3894(01)00311-9.

[59] Takahashi, N., Yoshida, T., Kojima, S., Yamaguchi, S., Ohtsuka, R., Takeda, M., et al., 2018. Pathological and clinical pathological changes induced by four-week, repeated-dose, oral administration of the wood preservative chromated copper arsenate in wistar rats. Toxicol Pathol 46 (3), 312–323. https://doi.org/10.1177/0192623318765392.

[60] Tanner, M., 2010. Shorter signals for improved signal to noise ratio, the influence of Poisson distribution. J Anal At Spectrom 25 (3), 405–407.

[61] Tavares, K.P., de Oliveira, Á.C., Vicentini, D.S., Melegari, S.P., Matias, W.G., Barbosa, S., et al., 2014. Acute toxicity of copper and chromium oxide nanoparticles to Daphnia similis. Ecotoxicol Environ Contam 9 (1), 43–50.

[62] Tou, F., Yang, Y., Feng, J., Niu, Z., Pan, H., Qin, Y., et al., 2017. Environmental risk implications of metals in sludges from waste water treatment plants: the discovery of vast stores of metal-containing nanoparticles. Environ Sci Technol 51 (9), 4831–4840.

[63] U. EPA, 2022. Chromated Arsenicals (CCA). https://www.epa.gov/ingredients-used-pesticide-products/chromated-arsenicals-cca.

[64] Van Der Werf, G.R., Randerson, J.T., Giglio, L., Van Leeuwen, T.T., Chen, Y., Rogers, B.M., et al., 2017. Global fire emissions estimates during 1997–2016. Earth Syst Sci Data 9 (2), 697–720.

[65] Wan, X., Li, C., Parikh, S.J., 2021. Chemical composition of soil-associated ash from the southern California Thomas Fire and its potential inhalation risks to farmworkers. J Environ Manag 278, 111570. https://doi.org/10.1016/j.jenvman.2020.111570.

[66] Wang, J., Nabi, M.D.M., Erfani, M., Goharian, E., Baalousha, M., 2022. Identification and quantification of anthropogenic nanomaterials in urban rain and runoff using single particle-inductively coupled plasma-time of flight-mass spectrometry. Enviro. Sci Nano 9, 714–729. https://doi.org/10.1039/D1EN00850A.

[67] Wasson, S.J., Linak, W.P., Gullett, B.K., King, C.J., Touati, A., Huggins, F.E., et al., 2005. Emissions of chromium, copper, arsenic, and PCDDs/Fs from open burning of CCA-treated wood. Environ Sci Technol 39 (22), 8865–8876. https://doi.org/10.1021/es050891g.

[68] M. Wibbenmeyer, A. McDarris, 2021. Wildfires in the United States 101: Context and Consequences. https://www.rff.org/publications/explainers/wildfires-in-the-united-states-101-context-and-consequences/. (Accessed 29 March 2022).

[69] Williams, A.P., Cook, E.R., Smerdon, J.E., Cook, B.I., Abatzoglou, J.T., Bolles, K., et al., 2020. Large contribution from anthropogenic warming to an emerging North American megadrought. Science 368 (6488), 314–318.

[70] Wotton, B.M., Gould, J.S., McCaw, W.L., Cheney, N.P., Taylor, S.W., 2011. Flame temperature and residence time of fires in dry eucalypt forest. Int J Wildland Fire 21 (3), 270–281.

[71] Yuan, W., Liu, X., Li, L., 2014. Synthesis, characterization and photocatalytic activity of cubic-like CuCr2O4 for dye degradation under visible light irradiation. Appl Surf Sci 319, 350–357.